Supporting Information

Miyashiro and Goulian 10.1073/pnas.0807278105

SI Text

Strain Construction. For lists of strains and plasmids, see Tables S1 and S2, respectively. For a list of primers used in their construction, see Table S3.

Fluorescent Reporters. The construction details of the CFP reporter used in this study have been described previously (1). Briefly, the *tetA* promoter was cloned upstream of *cfp* into pAH70 (2). In the absence of the repressor TetR, the *tetA* promoter is constitutively expressed (3, 4). The resulting plasmid (pTM27) was integrated into the chromosome of the *Escherichia coli* strain MG1655 at the HK phage attachment site as described in ref. 2, yielding TIM10. In some strains, the *kan* marker was removed as described in ref. 1 and are annotated as *attHK*::[pTM27 Δ*kan*] in Table S1.

The YFP reporter construct used in Figs. 1*C*, 3*A*, and 4*D* contains a transcriptional fusion of *yfp* to the *mgrB* operon. To construct this reporter, *yfp* with a ribosome binding site (5) was amplified from pMG32 by PCR using primers P01 and P02 and cloned into the SalI site of pKD13 (6), which contains the kanamycin resistance gene flanked by FRT sites. The *yfp-kan* cassette of this plasmid (pTM70) was amplified by PCR using primers P03 and P04, integrated into the chromosome downstream of *mgrB* via λ Red recombination, and introduced into a clean MG1655 background by P1 transduction. Expression of FLP recombinase as in ref. 6 removed the *kan* gene. The *cfp-kan* construct of TIM10 was introduced into this strain by P1 transduction to yield TIM39.

The construction details of the YFP reporter used in Figs. 3*B* and 4*C* have been previously described (1). Briefly, the *mgrB* promoter was cloned upstream of *yfp* into pCAH63 (2). The resulting plasmid (pTM79) was integrated into the chromosome of MG1655. The *cat* gene in the resulting strain was then replaced by a *kan* gene flanked by FRT sites by λ Red recombination. The reporter was subsequently moved into TIM64 by P1 transduction and the *kan* gene was removed by expression of FLP recombinase to yield TIM92.

Gene Deletions. We deleted *phoPphoQ* by λ Red recombination, replacing the *phoPphoQ* operon with a *cat* gene flanked by FRT sites that had been amplified from pKD3 by PCR using primers P05 and P06. The resultant construct was moved into various strain backgrounds using P1 transduction, and the *cat* gene was removed by expressing FLP recombinase.

In experiments that required the use of IPTG, we used Δ*lacZYA* strains, which avoided potential difficulties due to the presence of LacY (7). We deleted *lacZYA* by λ Red recombination, replacing the *lacZYA* operon with a *cat* gene flanked by FRT sites that had been amplified from pKD3 by PCR using primers P07 and P08. This construct was introduced by P1 transduction into particular strains, and the *cat* gene was removed by expressing FLP recombinase.

Nonautoregulated Strain. To remove the autoregulated P1 promoter, we used inverse PCR (8) with a plasmid containing the *phoPphoQ* operon and primers P09 and P10. This replaced the −10 region of the P1 promoter up to just before the PhoP ribosome binding site with a BamHI restriction site. This mutated *phoPphoQ* operon was amplified by PCR using primers P11 and P12, and cloned into pCAH63 digested with EcoRI and XmnI to yield pTM39. A wild-type control plasmid (pTM38) was also constructed by amplifying the wild-type *phoPphoQ* operon by PCR using primers P11 and P12, and cloning the product into pCAH63. The plasmids pTM38 and pTM39 were integrated into the chromosome at the lambda phage attachment (2) in an *mgrB* reporter strain that was deleted for *phoPphoQ*, to yield TIM44 and TIM45, respectively. In addition, the plasmids pTM38 and pTM39 were integrated into the chromosome of TIM13 to yield TIM68 and TIM69, respectively.

Plasmids pTM175 and pTM176 were constructed by amplifying the *phoPphoQ* operon with or without the P1 promoter by PCR using primers P09 and P10 from pTM38 and pTM39, respectively. The ends of the PCR products were phosphorylated by T4 polynucleotide kinase and ligated into an XbaI-BamHI vector fragment of pTM118 that was blunt ended with T4 DNA polymerase. These plasmids were integrated into the chromosome of TIM215 to yield TIM284 and TIM285, respectively.

IPTG-Inducible *phoPphoQ*. To control expression of *phoPphoQ*, the *phoPphoQ* operon with the wild-type ribosome binding sites were amplified from the chromosome of MG1655 using primers P13 and P12, and cloned into the plasmid pEB52 using XbaI and HindIII to yield pTM58. The plasmid pEB52 (Goulian lab stock) is a derivative of pTrc99A (9) in which the start codon at the beginning of the multicloning site was removed by digesting with NcoI, blunt ending with mung bean nuclease, and self-ligating. To lower the range of *phoPphoQ* expression, we also constructed pTM85 by weakening the −35 region of the *trc* promoter in pTM58 (denoted P_{trc}*) as described in ref. 10. The sequences ranging from $lacI^q$ thru *phoPphoQ* within pTM58 and pTM85 were then cloned into the plasmid pTM118 to yield pTM119 and pTM120, respectively. These plasmids were integrated into the chromosome at the Φ_{80} phage attachment site as in ref. 2. The integrated constructs were then moved by P1 transduction into TIM215, an *mgrB* reporter strain that contains Δ*phoPphoQ* and Δ*lacZYA* alleles, to yield TIM219 and TIM220, respectively.

phoQ(*T281R*) Constructs. To construct *phoQ*(*T281R*), site-directed mutagenesis was performed on a pEB52-derived plasmid containing *phoPphoQ* using primers P14 and P15. The mutation of cytosine to guanine at nucleotide 842 results in a threonine-to-arginine mutation in PhoQ at residue 281. The sequence spanning $lacI^q$ to *phoPphoQ*(*T281R*) was amplified using primers P16 and P17, digested with PstI and SalI, and cloned into the PstI-SalI vector fragment of pTM118. The resulting plasmid (pTM168) was integrated into the chromosome of TIM215 to yield TIM270.

To construct pTM177 and pTM178, a fragment of *phoQ*(*T281R*) (containing the T281R mutation and C terminus) was cloned into the DraIII-XmnI vector fragments of pTM175 and pTM176. These plasmids were integrated into the chromosome of TIM215 to yield TIM286 and TIM287.

Plasmids for Protein Purification. To construct the plasmids for the expression of $PhoQ_{cyt}$-6xHis and $PhoQ(T281R)_{cyt}$-6xHis, primers P19 and P20 were used with templates pTM58 and pTM168 to amplify the cytoplasmic domains of *phoQ* and *phoQ*(*T281R*), respectively. The products were digested with NdeI and HindIII, and ligated to the NdeI-HindIII vector fragment of pET22b, resulting in pAN1 and pTM154, respectively.

Note that all integrations at phage att sites were verified to be in single copy by PCR (2).

Model of Two-Component Signaling with a Bifunctional Histidine Kinase

Autoregulation Module. Because we are modeling only the steady-state behavior of the circuit, we use a simplified model in which the rate of protein production is a saturating function of the concentration of phosphorylated response regulator ([RR-P]). We therefore take the total cellular concentration of response regulator to satisfy

$$\frac{d[\mathrm{RR}]_{\mathrm{total}}}{dt} = B + \frac{A[\mathrm{RR-P}]}{D + [\mathrm{RR-P}]} - \frac{[\mathrm{RR}]_{\mathrm{total}}}{\tau},$$

where B parametrizes the basal production, A and D parameterize the [RR-P]-dependent production, and τ is determined by protein degradation or dilution from cell doubling. One could more generally allow for cooperativity in the dependence on [RR-P] by choosing a sigmoidal saturating function (i.e., a Hill coefficient greater than 1). However, the qualitative conclusions of the model do not change except in the limit of a very steep sigmoidal function, where bistability can emerge. Because we have not observed any evidence of such bistability in any of our single-cell measurements, we do not consider this possibility any further here. To describe the steady state, we set the time derivative to 0 in the above expression, which gives

$$[\mathrm{RR}]_{\mathrm{total}} = \tau B + \frac{\tau A[\mathrm{RR-P}]}{D + [\mathrm{RR-P}]} \qquad \textbf{[1]}$$

We assume that the total amount of histidine kinase ($[\mathrm{HK}]_{\mathrm{total}}$), whose gene is in an operon with the gene for the response regulator, is at least roughly proportional to $[\mathrm{RR}]_{\mathrm{total}}$. As is evident hereafter, small changes in $[\mathrm{HK}]_{\mathrm{total}}$ relative to $[\mathrm{RR}]_{\mathrm{total}}$ will not be important.

Phosphorylation Cycle. The phosphorylation cycle shown in Fig. 2*B* of the main text and in Fig. S1 is based on a model described previously (5). The Michaelis constants for the phosphatase and phosphotransfer reactions are related to the concentrations of reaction intermediates by

$$\frac{[\mathrm{RR-P}][\mathrm{HK}]}{[(\mathrm{RR-P})\mathrm{HK}]} = \mathrm{K_{Mp}} \frac{[\mathrm{RR}][\mathrm{HK-P}]}{[\mathrm{RR}(\mathrm{HK-P})]} = \mathrm{K_{Mt}}$$

At steady state, the rates of production and loss must balance for [RR-P]:

$$k_{\mathrm{p}}[(\mathrm{RR-P})\mathrm{HK}] = k_{\mathrm{t}}[\mathrm{RR}(\mathrm{HK-P})]$$

and for [HK-P]:

$$k_{\mathrm{k}}[\mathrm{HK}] = k_{-k}[\mathrm{HK-P}] + k_{\mathrm{t}}[\mathrm{RR}(\mathrm{HK-P})].$$

Substituting into these expressions the above relations for the Michaelis constants gives

$$k_{\mathrm{p}}\frac{[\mathrm{RR-P}][\mathrm{HK}]}{\mathrm{K_{Mp}}} = k_{\mathrm{t}}\frac{[\mathrm{RR}][\mathrm{HK-P}]}{\mathrm{K_{Mt}}}$$

$$k_{\mathrm{k}}[\mathrm{HK}] = k_{-\mathrm{k}}[\mathrm{HK-P}] + k_{\mathrm{t}}\frac{[\mathrm{RR}][\mathrm{HK-P}]}{\mathrm{K_{Mt}}}.$$

Combining these two equations then gives

$$\frac{\mathrm{C_p}}{[\mathrm{RR-P}]} = \frac{\mathrm{C_t}}{[\mathrm{RR}]} + 1,$$

where $\mathrm{C_p} = k_{\mathrm{k}}K_{\mathrm{Mp}}/k_{\mathrm{p}}$ and $\mathrm{C_t} = k_{-\mathrm{k}}K_{\mathrm{Mt}}/k_{\mathrm{t}}$. We assume that the concentrations of the reaction intermediates (RR-P)HK and RR(HK-P) are small compared with the concentrations of RR and RR-P. This will be the case if $[\mathrm{RR}]_{\mathrm{total}} > [\mathrm{HK}]_{\mathrm{total}}$, which holds for at least two systems: PhoQ/PhoP (T.M. and M.G., unpublished data) and EnvZ/OmpR (12). We therefore take $[\mathrm{RR}]_{\mathrm{total}} \approx [\mathrm{RR}]+[\mathrm{RR-P}]$. Combining this with the previous relation gives [RR-P] in terms of $[\mathrm{RR}]_{\mathrm{total}}$:

$$[\mathrm{RR-P}] \approx \frac{1}{2}(C_{\mathrm{t}} + \mathrm{C_p} + [\mathrm{RR}]_{\mathrm{total}}) - \frac{1}{2}\sqrt{(\mathrm{C_t} + \mathrm{C_p} + [\mathrm{RR}]_{\mathrm{total}})^2 - 4\mathrm{C_p}[\mathrm{RR}]_{\mathrm{total}}}. \qquad \textbf{[2]}$$

This gives the saturating curve shown in Fig. 2*B* in the main text.

The choice of the root in Eq. **2** is fixed by the requirement: $[\mathrm{RR-P}] \leq [\mathrm{RR_{total}}]$. For the special case of $\mathrm{C_t} = 0$, which occurs when $k_{-\mathrm{k}} = 0$, the correct root depends on the value of $[\mathrm{RR}]_{\mathrm{total}}$. For $[\mathrm{RR}]_{\mathrm{total}} > \mathrm{C_p}$, the negative root must be taken, which gives $[\mathrm{RR-P}] = \mathrm{C_p}$. For $[\mathrm{RR}]_{\mathrm{total}} < \mathrm{C_p}$, one must instead take the positive root, which gives $[\mathrm{RR-P}] = [\mathrm{RR}]_{\mathrm{total}}$ (i.e., the response regulator is fully phosphorylated). This limit is discussed in more detail in a related model in ref. 13.

Steady-State Solution. Eqs. **1** and **2** are plotted in the main text in Fig. 2 *A* and *B*, respectively, with $\tau B = 15$, $\tau A = 45$, $D = 40$, and $\mathrm{C_p} = 10$ or 30 as indicated. All concentrations are measured in units of $\mathrm{C_t}$. These parameters were chosen to show the qualitative features of the model. The steady-state level of [RR-P] in the autoregulated system is given by the unique solution to Eqs. **1** and **2**. This solution can be found graphically, as indicated in Fig. 2*C*, or numerically, which is shown in Fig. S2 with the above parameters for the autoregulated model and with $\tau A = 0$ for the non-autoregulated model. A comparison of the autoregulated circuit with the non-autoregulated version shows the stimulus-dependent amplification provided by autoregulation (Fig. S2). Both circuits have similar stimulus-response curves for the low range of stimuli. However, at high stimulus the output from the non-autoregulated circuit begins to roll off as the pool of unphosphorylated response regulator becomes depleted. Autoregulation preempts this roll-off by increasing the response regulator pool. The corresponding sensitivities of the outputs as a function of $\mathrm{C_p}$ for the autoregulated and non-autoregulated models are shown in Fig. S3.

Growth-Limiting Mg^{2+} Conditions. As described in the main text, PhoP-regulated transcription is strongly activated by conditions of very low magnesium. The strong induction of PhoP-regulated genes required both PhoQ and PhoP (data not shown). In addition, we found that when we slightly increased the starting concentration of magnesium, the sharp increase in transcription was delayed (Fig. S4). These findings suggest that the high induction level is due to strong stimulation of PhoQ as cells deplete magnesium from the growth medium.

Although these conditions do not correspond to balanced growth, we were able to produce a short plateau in the induction curve by using a large excess of filtered medium isolated from a culture grown to an intermediate time point (Fig. S5). This indicates that under these growth conditions, the PhoQ/PhoP system is in a quasi-steady state; the time scales for reaching steady-state levels of PhoP-P and steady-state PhoP-regulated transcription are apparently faster than the time scale associated with changes in PhoQ stimulation due to magnesium depletion of the medium from cell growth.

1. Miyashiro T, Goulian M (2007) Stimulus-dependent differential regulation in the Escherichia coli PhoQ PhoP system. *Proc Natl Acad Sci USA* 104:16305–16310.
2. Haldimann A, Wanner BL (2001) Conditional-replication, integration, excision, and retrieval plasmid-host systems for gene structure-function studies of bacteria. *J Bacteriol* 183:6384–6393.
3. Hillen W, Berens C (1994) Mechanisms underlying expression of Tn10 encoded tetracycline resistance. *Annu Rev Microbiol* 48:345–369.
4. Miyashiro T, Goulian M (2007) Single-cell analysis of gene expression by fluorescence microscopy. *Methods Enzymol* 423:458–475.
5. Batchelor E, Goulian M (2003) Robustness and the cycle of phosphorylation and dephosphorylation in a two-component regulatory system. *Proc Natl Acad Sci USA* 100:691–696.
6. Datsenko KA, Wanner BL (2000) One-step inactivation of chromosomal genes in Escherichia coli K-12 using PCR products. *Proc Natl Acad Sci USA* 97:6640–6645.
7. Khlebnikov A, Keasling JD (2002) Effect of lacY expression on homogeneity of induction from the P(tac) and P(trc) promoters by natural and synthetic inducers. *Biotechnol Prog* 18:672–674.
8. Ochman H, Gerber AS, Hartl DL (1988) Genetic applications of an inverse polymerase chain reaction. *Genetics* 120:621–623.
9. Amann E, Ochs B, Abel KJ (1988) Tightly regulated tac promoter vectors useful for the expression of unfused and fused proteins in Escherichia coli. *Gene* 69:301–315.
10. Weiss DS, Chen JC, Ghigo JM, Boyd D, Beckwith J (1999) Localization of FtsI (PBP3) to the septal ring requires its membrane anchor, the Z ring, FtsA, FtsQ, and FtsL. *J Bacteriol* 181:508–520.
11. Skerker JM, *et al.* (2008) Rewiring the specificity of two-component signal transduction systems. *Cell* 133:1043–1054.
12. Cai SJ, Inouye M (2002) EnvZ-OmpR interaction and osmoregulation in Escherichia coli. *J Biol Chem* 277:24155–24161.
13. Shinar G, Milo R, Martinez MR, Alon U (2007) Input output robustness in simple bacterial signaling systems. *Proc Natl Acad Sci USA* 104:19931–19935.

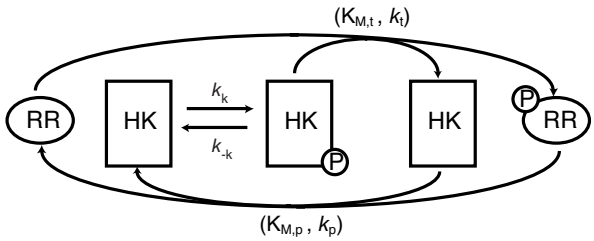

Fig. S1. A generalized version of the phosphorylation cycle described in the main text labeled with rate constants for autophosphorylation, phosphotransfer, and phosphatase reactions.

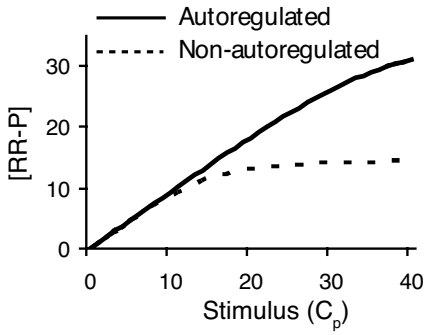

Fig. S2. Autoregulation boosts the response range at high stimulus. The steady-state level of phosphorylated response regulator is plotted as a function of the input stimulus (parameterized by C_p) for the autoregulated and non-autoregulated circuits. See *SI Text* for parameter values.

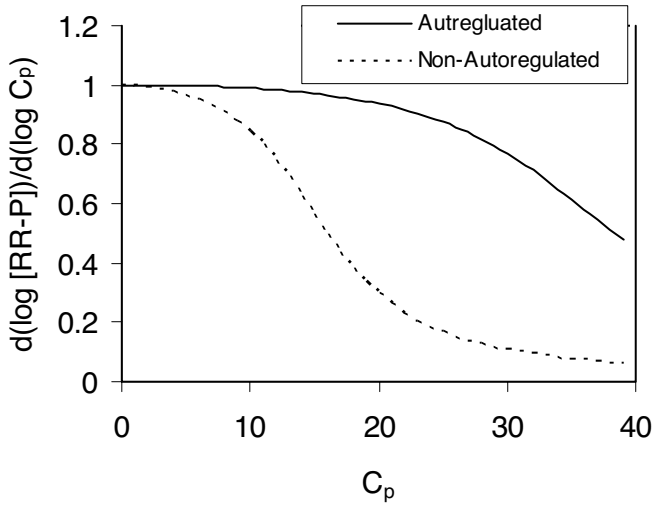

Fig. S3. Comparison of the sensitivity of the output ([RR-P]) to changes in C_p for the autoregulated and non-autoregulated models. The sensitivity, which is the fractional change in [RR-P] relative to (and resulting from) a fractional change in C_p, is given by

$$\frac{d\ \log[\mathrm{RR}-\mathrm{P}]}{d\ \log \mathrm{C_p}} = \frac{\mathrm{C_p}}{[\mathrm{RR}-\mathrm{P}]}\frac{d[\mathrm{RR}-\mathrm{P}]}{d\mathrm{C_p}}.$$

The curves were derived from the solutions plotted in Fig. S2.

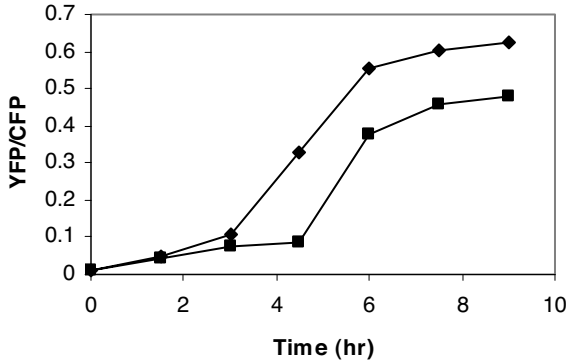

Fig. S4. The onset of high PhoP-regulated transcription is Mg^{2+} dependent. The YFP/CFP fluorescence ratio of an *mgrB* reporter strain (TIM44) was measured at the indicated times. Overnight cultures (grown in 1 mM Mg^{2+}) were diluted 1:1,000 into minimal media without added Mg^{2+} (diamonds) or with 10 μM Mg^{2+} (squares). At the final time points, the cells have stopped growing, presumably due to low levels of Mg^{2+}. Thus, the observed difference between the final YFP/CFP ratios is most likely due to differences in magnesium depletion rates for the two cultures.

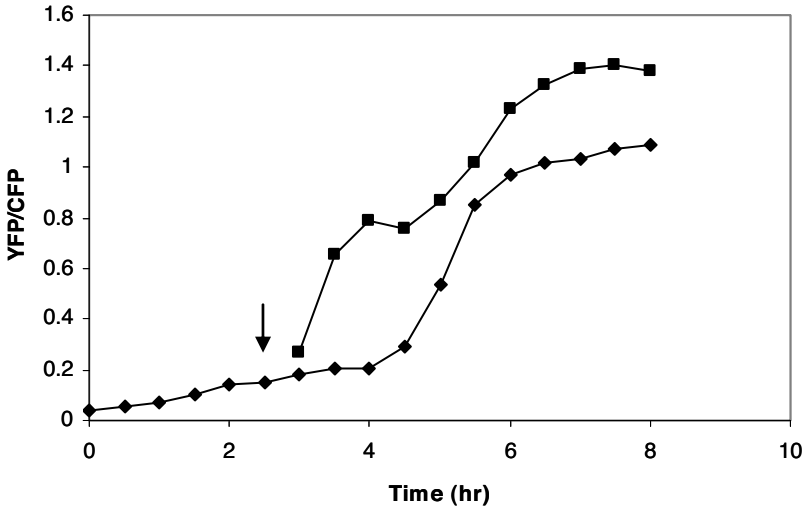

Fig. S5. PhoQ/PhoP-regulated transcription under conditions of very low magnesium are quasi-steady state. The YFP/CFP fluorescence ratio of an *mgrB* reporter strain (TIM44) was measured at the indicated time points. An overnight culture was diluted into medium without magnesium (diamonds). At the time indicated by the arrow, a sample was used to inoculate spent medium (squares). The spent medium was obtained by filter-sterilizing supernatant from a culture grown in the absence of magnesium for 5.5 h.

Table S1. Strains

Strain	Relevant genotype	Reference
BL21(DE3)	*E. coli* host for protein expression	Novagen
MG1655	*rph-1*	*E. coli* Genetic Stock Center, CGSC no. 7740
TIM10	MG1655 *att*λ::pTM27	(1)
TIM13	MG1655 Δ(*P2P1-phoPphoQ*)	This work
TIM39	MG1655 Φ(*mgrB*$^{+}$-*yfp*$^{+}$) *attHK*::pTM27	This work
TIM42	MG1655 Δ(*P2P1-phoPphoQ*) Φ(*mgrB*$^{+}$–*yfp*$^{+}$) *attHK*::pTM27	This work
TIM44	MG1655 Δ(*P2P1-phoPphoQ*) Φ(*mgrB*$^{+}$–*yfp*$^{+}$) *att*λ::pTM38 *attHK*::pTM27	This work
TIM45	MG1655 Δ(*P2P1-phoPphoQ*) Φ(*mgrB*$^{+}$–*yfp*$^{+}$) *att*λ::pTM39 *attHK*::pTM27	This work
TIM64	MG1655 *attHK*::[pTM27 Δ*kan*]	(1)
TIM68	MG1655 Δ(*P2P1-phoPphoQ*) *att*λ::pTM38	This work
TIM69	MG1655 Δ(*P2P1-phoPphoQ*) *att*λ::pTM39	This work
TIM92	MG1655 *att*λ::[pTM79 Δ*cat*] *attHK*::[pTM27 Δ*kan*]	(1)
TIM210	MG1655 Δ*lacZYA att*λ:: [pTM79 Δ*cat*] *attHK*::[pTM27 Δ*kan*]	This work
TIM215	MG1655 Δ(*P2P1-phoPphoQ*) Δ*lacZYA att*λ:: [pTM79 Δ*cat*] *attHK*::[pTM27 Δ*kan*]	This work
TIM219	MG1655 Δ(*P2P1-phoPphoQ*) Δ*lacZYA att*λ:: [pTM79 Δ*cat*] *attHK*::[pTM27 Δ*kan*] *att*Φ_{80}::*pTM119*	This work
TIM220	MG1655 Δ(*P2P1-phoPphoQ*) Δ*lacZYA att*λ:: [pTM79 Δ*cat*] *attHK*::[pTM27 Δ*kan*] *att*Φ_{80}::*pTM120*	This work
TIM270	MG1655 Δ(*P2P1-phoPphoQ*) Δ*lacZYA att*λ:: [pTM79 Δ*cat*] *attHK*::[pTM27 Δ*kan*] *att*Φ_{80}::*pTM168*	This work
TIM284	MG1655 Δ(*P2P1-phoPphoQ*) Δ*lacZYA att*λ:: [pTM79 Δ*cat*] *attHK*::[pTM27 Δ*kan*] *att*Φ_{80}::*pTM175*	This work
TIM285	MG1655 Δ(*P2P1-phoPphoQ*) Δ*lacZYA att*λ:: [pTM79 Δ*cat*] *attHK*::[pTM27 Δ*kan*] *att*Φ_{80}::*pTM176*	This work
TIM286	MG1655 Δ(*P2P1-phoPphoQ*) Δ*lacZYA att*λ:: [pTM79 Δ*cat*] *attHK*::[pTM27 Δ*kan*] *att*Φ_{80}::*pTM177*	This work
TIM287	MG1655 Δ(*P2P1-phoPphoQ*) Δ*lacZYA att*λ:: [pTM79 Δ*cat*] *attHK*::[pTM27 Δ*kan*] *att*Φ_{80}::*pTM178*	This work

Table S2. Plasmids

Plasmid	Relevant genotype	Reference
pAH70	*ori*$R_{\gamma R6K}$ *kan att*P_{HK} P_{syn1}-*pstS**	(2)
pAN1	pET22b $PhoQ_{cyt}$-6xHis expression vector	This work
pCAH63	*ori*$R_{\gamma R6K}$ *cat att*P_{λ} *Psyn1-uidAf*	(2)
pET22b	protein expression vector	Novagen
pInt-ts	λ*cI857*(ts), λ*pR-xis*, *bla*(ApR), *int*$_{\lambda pR'}$ *repA101*(ts)	(2)
pKD3	*ori*$R_{\gamma R6K}$ *bla FRT*::*cat*::*FRT*	(6)
pKD4	*ori*$R_{\gamma R6K}$ *bla FRT*::*kan*::*FRT*	(6)
pKD13	*ori*$R_{\gamma R6K}$ *bla FRT*::*kan*::*FRT*	(6)
pMG32	*bla yfp*	Lab stock
pMG34	*bla cfp*	Lab stock
pTM27	pAH70 P_{tetA}-*cfp*	(1)
pTM38	pCAH63 Δ(P_{syn1}-*uidAf*) *P2P1-phoPphoQ*	This work
pTM39	pCAH63 Δ(P_{syn1}-*uidAf*) *P2-phoPphoQ*	This work
pTM50	pET22b PhoP-6xHis expression vector	(1)
pTM58	pTrc99A *lacI*^{q} P_{trc}-*phoPphoQ*	This work
pTM70	pKD13 *yfp*	This work
pTM79	pCAH63 P_{mgrB}-*yfp*	(1)
pTM85	pTrc99A *lacI*^{q} P_{trc*}-*phoPphoQ*	This work
pTM118	*ori*$R_{\gamma R6K}$ *cat att*$P_{\Phi 80}$ *Psyn1--uidAf*	This work
pTM119	pTM118 Δ(P_{syn1}-*uidAf*) *lacI*^{q} P_{trc}-*phoPphoQ*	This work
pTM120	pTM118 Δ(P_{syn1}-*uidAf*) *lacI*^{q} P_{trc*}-*phoPphoQ*	This work
pTM154	pET22b $PhoQ(T281R)_{cyt}$-6xHis expression vector	This work
pTM168	pTM118 Δ(P_{syn1}-*uidAf*) *lacI*^{q} P_{trc}-*phoPphoQ(T281R)*	This work
pTM175	pTM118 $P_2P_{1\text{-}phoPphoQ}$	This work
pTM176	pTM118 P_2-*phoPphoQ*	This work
pTM177	pTM118 $P_2P_{1\text{-}phoPphoQ(T281R)}$	This work
pTM178	pTM118 P_2-*phoPphoQ(T281R)*	This work
pTrc99A	*lacI*^{q} P_{trc}-MCS *bla*	(9)
p(6xHis-MBP-EnvZ + MI + loop5)	Expression plasmid for an EnvZ chimera that phosphorylates PhoP.	(11)

Table S3. Primers

Primer name	Sequence
P01	ATCTCGAGTTCACACAGGAAACAGCTATG
P02	CCGTCGACCAGGTCAGCTAATTAAGC
P03	AATTTTTCAGCGGAATTTGTGCCATTAACCAGTTTATCCCGTGGTGATATGTGTAGGCTGGAGCTGCTTC
P04	GAGTAGAGGCGCTATTCTACCACTGCTGGAGAGGAAGAAAATCTAGTGCTCTTCGTCTGTTTCTACTGGT
P05	ACCTCGTATCAGTGCCGGATGGCGATGCTGTCCGGCCTGCTTATTAAGATGTGTAGGCTGGAGCTGCTTCG
P06	TTATTCATCTTTCGGCGCAGAATGCTGGCGACCAAAAATCACCTCCATCCCATATGAATATCCTCCTTAG
P07	GGAAACAGCTATGACCATGATTACGGATTCACTGGCCGTCGTTTTACAAGTGTAGGCTGGAGCTGCTTC
P08	ATTTAAACTGACGATTCAACTTTATAATCTTTGAAATAATAGTGCTTATCATGAATATCCTCCTTAGTTC
P09	GGGGATCCTAAGACAGGGAGAAATAAAA
P10	GGGGATCCGGTTATGGGGGTAAACATTA
P11	GGGAATTCGTATCAGTGCCGGATGG
P12	CAAAGCTTGCGTGAAGTATGGGCATATT
P13	GACAGGGAGAAATAAAAATGCGCGT
P14	ACCCATAGTCTGAAAAGGCCACTGGCGGTGCTG
P15	CAGCACCGCCAGTGGCCTTTTCAGACTATGGGT
P16	GTACTGCAGGCAGCAGATCAATTCGCG
P17	GCGGTCGACTTGCGTGAAGTATGGGCAT
P18	AGATATACATATGCCCATCGAAGCCCTGGCAAA
P19	CCCAAGCTTTTCATCTTTCGGCGCAGAAT